Science of the Total Environment 855 (2023) 158655

Contents lists available at ScienceDirect

Science of the Total Environment

journal homepage: www.elsevier.com/locate/scitotenv

Organic aerosol sources in Krakow, Poland, before implementation of a solid fuel residential heating ban

Roberto Casotto [a], Alicja Skiba [b], Martin Rauber [c], Jan Strähl [c], Anna Tobler [a,d], Deepika Bhattu [a,1], Houssni Lamkaddam [a], Manousos I. Manousakas [a], Gary Salazar [c], Tianqu Cui [a], Francesco Canonaco [d], Lucyna Samek [e], Anna Ryś [e], Imad El Haddad [a], Anne Kasper-Giebl [f], Urs Baltensperger [a], Jaroslaw Necki [b], Sönke Szidat [c], Katarzyna Styszko [g], Jay G. Slowik [a], André S.H. Prévôt [a,*], Kaspar R. Daellenbach [a,*]

[a] Laboratory of Atmospheric Chemistry, Paul Scherrer Institute, 5232 Villigen-PSI, Switzerland
[b] Department of Applied Nuclear Physics, Faculty of Physics and Applied Computer Science, AGH University of Science and Technology, Kraków, Poland
[c] Department of Chemistry, Biochemistry and Pharmaceutical Sciences & Oeschger Centre for Climate Change Research, University of Bern, 3012 Bern, Switzerland
[d] Datalystica Ltd., Park innovAARE, 5234 Villigen, Switzerland
[e] Department of Medical Physics and Biophysics, Faculty of Physics and Applied Computer Science, AGH University of Science and Technology, Kraków, Poland
[f] Institute for Chemical Technologies and Analytics, Vienna University of Technology, 1060 Vienna, Austria
[g] Department of Coal Chemistry and Environmental Sciences, Faculty of Energy and Fuels, AGH University of Science and Technology, Kraków, Poland

HIGHLIGHTS

- We determine the organic aerosol sources in Krakow, a pollution hotspot in Europe.
- Direct emissions from residential heating coal combustion strongly impacts OA in winter (making it largely water-insoluble).
- Secondary OA is strongly impacted by fossil fuel combustion emissions in winter and largely biogenic in summer.

GRAPHICAL ABSTRACT

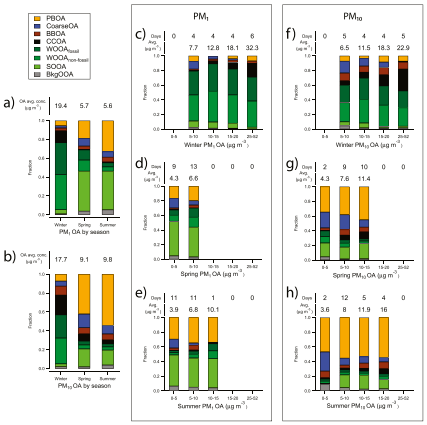

ARTICLE INFO

Editor: Pingqing Fu

Keywords:
Coal combustion
Fossil carbon
Source apportionment
PMF
OA

ABSTRACT

Krakow is a pollution hot-spot in Europe which is thought to be caused mainly by a high use of coal combustion (power plants, residential heating). Here, we quantify the impact of coal burning on air quality in the city of Krakow before the use of solid fuels for residential heating was banned within the city of Krakow. The particulate matter (PM) was collected on 126 24-hour filter samples (January to September, both PM_1 and PM_{10}, i.e., with an aerodynamic diameter smaller than 1 μm and 10 μm, respectively) and analyzed with an aerosol mass spectrometer and the sources of the organic aerosol (OA) quantified. Secondary OA (SOA) likely from residential heating was the main contributor to winter-time OA (78 % in PM_1, 57 % in PM_{10}) and was composed of equal parts of fossil and non-fossil emissions. Additionally, fresh solid fuel combustion emissions from residential heating contributed to OA during winter (coal combustion OA (CCOA): 12 %, biomass burning OA (BBOA): 3 %). While BBOA contributed substantially to water-soluble OA, COOA

* Corresponding authors.
E-mail addresses: andre.prevot@psi.ch (A.S.H. Prévôt), kaspar.daellenbach@psi.ch (K.R. Daellenbach).
[1] Now at Department of Civil and Infrastructure Engineering, Indian Institute of Technology Jodhpur, Jodhpur 342037, India.

http://dx.doi.org/10.1016/j.scitotenv.2022.158655
Received 18 March 2022; Received in revised form 31 August 2022; Accepted 6 September 2022
Available online 8 September 2022

was found to be water-insoluble and thus not identified as part of water-soluble OA. Together with the fairly low water-solubility of winter oxygenated OA (WOOA, 29 %), this leads to a low overall water-solubility of organic carbon during winter (35 %). In contrast, spring and summer were characterized by more soluble organic carbon (71 % in PM_1, 55 % in PM_{10}) which was dominated by biogenic sources (non-fossil), i.e., fine biogenic secondary oxygenated OA (summer oxygenated OA (SOOA): 35 % in PM_1) and coarse primary biological OA (PBOA: 54 % in PM_{10}). Overall, here we provide information on OA's sources needed to evaluate the success of mentioned efforts to improve air quality in Krakow in future studies.

1. Introduction

Atmospheric aerosols have a negative effect on human health, causing an estimated 3.3 million annual premature deaths worldwide (Burnett et al., 2018; IPCC, 2014; WHO, 2018). Organic aerosols (OA) contribute substantially to the aerosol concentration, especially in cities and nearby areas (Jimenez et al., 2009) and are thought to be particularly harmful to human health (Daellenbach et al., 2020). OA is composed of both natural sources, including plant emissions and plant debris, and anthropogenic sources such as vehicular emissions and solid fuel combustion. Source apportionment analyses relying on statistical un-mixing models, such as positive matrix factorization (PMF), separate OA into sources. Primary OA (POA) is directly emitted from, e.g., residential heating appliances (biomass burning OA: BBOA; coal combustion OA: CCOA) or traffic (hydrocarbon-like OA: HOA). Secondary OA (SOA) is formed in the atmosphere by reactions of gas-phase emissions. Understanding the OA sources is of prime importance to inform the general public and policy makers in order to manage public health risks. In 2021, the World Health Organization published new recommendations on air quality guideline (AQG) levels. These included new AQG levels for $PM_{2.5}$ and PM_{10} (particulate matter with an aerodynamic diameter smaller than 2.5 and 10 μm, respectively) where the recommended value for $PM_{2.5}$ was decreased from 10 to 5 μg m^{-3} and for PM_{10} from 20 to 15 μg m^{-3} (WHO, 2006; WHO, 2021). If implemented, these guidelines can further increase life expectancy (Kiesewetter et al., 2015). They also highlight the need for accurate knowledge on the PM sources. $PM_{2.5}$ concentrations are gradually but steadily decreasing in Europe, although substantial regional differences in both pollution levels and state of knowledge exist, and most regions are still well above these new AQG levels (Barmpadimos et al., 2012; Beloconi and Vounatsou, 2021).

Krakow is considered to be a pollution hotspot in Europe (Samek et al., 2020a). This is predominantly due to a high consumption of coal for energy production (some of the most polluting coal power plants are found in Poland (Grant et al., 2021)) and for residential heating (Stala-Szlugaj, 2018). The city of Krakow lies on the border of the Upper Silesian Coal Basin, one of the major coal production areas in the world (Bibler et al., 1998). The city is also prone to air pollution accumulation due to its topographical location (located inside a basin) which prevents ventilation. During the winter period, residential heating adds to air pollution substantially, causing air quality to deteriorate drastically (Fabiańska et al., 2016; Górka et al., 2020; Junninen et al., 2009). In Poland, the amount of air pollution has been decreasing during the past decades, but it still remains concerningly high in urban areas (Choi et al., 2015), impacting the health of the population (Gruszecka-Kosowska, 2018). Previous studies on sources of organic aerosol all show a high contribution of coal combustion in Poland, including Krakow and other cities in the south of the country (Almeida et al., 2020; Błaszczak and Mathews, 2020; Błaszczak et al., 2020; Górka et al., 2014; Kristensson et al., 2020; Szramowiat et al., 2016). Only few in-depth studies of OA source apportionment were performed in Krakow over a long period of time. The most recent one, by Tobler et al. (2021), used an online aerosol chemical speciation monitor (ACSM) and was able to apportion the OA into four time-dependent different sources. However, the ACSM has a much lower ion mass resolution than the aerosol mass spectrometer (AMS) used in this work, which limited the resolving power of the source apportionment.

In this study, we quantify the OA sources of PM_1 and PM_{10} during 2018, which represents the last winter residential solid fuel combustion was allowed inside Krakow city limits. We document the status before the new policies were implemented, allowing for the verification of their success in future years.

2. Methodology

2.1. Filter collection campaign

PM_1 and PM_{10} samples were collected on the roof of the Physics and Applied Computer Science Faculty of the AGH University building in Krakow, approximately 20 m above the ground. The site is urban, 2 km west of the Krakow city center. Krakow is characterized by cold winters, during which coal combustion for residential heating is a major contributor to the city's aerosol load (Tobler et al., 2021).

Aerosol was sampled between January 2018 and September 2018 every 4th day for 24 h (midnight to midnight) on pre-combusted (at 450 °C for 4 h) quartz fiber filters (Tissuequartz 2500 Qat-Up 150 mm, Pall Corporation) using two high-volume samplers (DHA-80 and DHA-80-C, DIGITEL AG). The filters were wrapped in aluminum foil and stored in plastic zip-lock bags at −21 °C. Field blanks were collected following the same protocol. The filter samples were transported inside polystyrene thermos-boxes and kept at low temperatures with cool packs pre-cooled at −21 °C.

2.2. Instrumentation and chemical analyses

2.2.1. Offline AMS and WSOC analyses

The concentration of water soluble organic carbon (WSOC) and the chemical composition were determined for 63 PM_1 and 63 PM_{10} ambient filter samples and for 12 field blank filters. A long time-of-flight aerosol mass spectrometer (L-ToF-AMS, Aerodyne) was used to characterize the chemical composition of the water-soluble organic species collected on the filters. The off-line measurement and analysis procedure is based on the analytical framework developed for the ToF-AMS by Daellenbach et al. (2016) and Bozzetti et al. (2017b), of which a brief description is given here. PM on a small fraction of the filter sample (area 2.5 cm^2) was extracted in 10 mL of ultra-pure water (Milli-Q®, 18.2 MΩ·cm at 25 °C, total organic carbon, TOC < 5 ppb, Merck Millipore), sonicated at 30 °C for 20 min and then vortexed for 60 s. The extract was filtered through a nylon membrane with 0.45 μm pores (Infochroma AG, Yeti HPLC filters, 13 mm diameter) in order to remove the residual material of the filter and larger insoluble particles to avoid clogging of the nebulizer or mass spectrometer inlets during the measurements. Each sample was spiked with 0.1 mL of 200 ppm solutions of isotopically-labelled ammonium sulfate $(NH_4)_2^{34}SO_4$ and ammonium nitrate $NH_4^{15}NO_3$. The extract was then nebulized (using an Apex nebulizer) with argon gas (99.999 % purity, PanGas AG), and the generated aerosol dried in a Nafion™ dryer (Perma Pure™), and sampled by the L-ToF-AMS. A mass spectrum was acquired every 36.5 s. The nebulization and measurement of each sample lasted 480 s, leading to approximately 15 usable mass spectra acquired per sample. Preceding each sample measurement, measurements of mass spectra of ultrapure water blanks were performed for 720 s to clean the lines connecting the nebulizer to the mass spectrometer inlet and to obtain a baseline for the sample measurements.

The analysis of the AMS dataset is based on the method developed by Daellenbach et al. (2016). Raw AMS data was processed using SQUIRREL (SeQUential Igor data RetRiEvaL v. 1.63; D. Sueper, University of Colorado, Boulder, CO, USA) and PIKA (Peak Integration and Key Analysis v. 1.23) to

obtain mass spectra of identified ions over the mass to charge (m/z) range 12–120. 482 organic fragment ions were identified in PIKA. The CO_2^+ peak and the related peaks of CO^+, H_2O^+, HO^+, and O^+ were corrected for NO_3^- induced artifacts by adapting the AMS fragmentation table using pure ammonium nitrate measurements (Daellenbach et al., 2017; Pieber et al., 2016). The following equation was used to correct the measured CO_2^+ to the real estimate:

$$CO_{2,real} = CO_{2,meas} - \left(\frac{CO_{2,meas}}{NO_{3,meas}}\right)_{NH_4NO_{3,pure}} \cdot \left(NO_{3,meas} + {}^{15}NO_{3,meas}\right) \quad (1)$$

Because H_2O^+, HO^+, CO^+, and O^+ are not directly measured but rather calculated as a constant fraction of CO_2^+, they were excluded from the PMF input and later re-calculated based on the CO_2^+ ion result.

The PIKA software outputs the raw data measurements and the minimum error time series which accounts for electronic noise and ion-to-ion variability at the detector ($m_{i,j}^{raw}$ and δ_i, where i is the instrument time index and j the ion index). The matrix elements $m_{i,j}^{raw}$ and δ_i were used to calculate the final matrix elements $m_{i,j}^{PMF}$ and corresponding error matrix elements $\sigma_{\alpha,j}^{PMF}$. Here, the index α runs over the $N_{Filters} = 138$ filters considered, which include the 12 field blanks (FBs). To each filter α corresponds a number N_{Filter_α} of mass spectra of filter-sample (denoted with indices $i \in Filter_\alpha$) and a number N_{Blank_α} of preceding water-blank measurements (denoted with indices $i \in Blank_\alpha$). The spectra, representing the water soluble organic aerosol (WSOA) concentration of the collected particles, were determined as

$$m_{\alpha,j}^{offline} = S_{\alpha,j}^{Filter_\alpha} - S_{\alpha,j}^{Blank_\alpha} = \frac{\sum_{i \in Filter_\alpha} m_{i,j}^{raw}}{N_{Filter_\alpha}} - \frac{\sum_{i \in Blank_\alpha} m_{i,j}^{raw}}{N_{Blank_\alpha}}. \quad (2)$$

where each $S_{\alpha,j}$ corresponds to the average of elements $m_{i,j}^{raw}$ over the corresponding subset of measurements. The error $\sigma_{\alpha,j}^{offline}$ associated with each ion signal was determined in two steps. First the standard deviation of the aforementioned averages was calculated. Second, the standard deviations were compared to the minimum error $\delta_{\alpha,j}$, which was derived from the PIKA δ_i output by correcting for m/z and integration time (Ulbrich et al., 2009). The higher value between the two was considered as error $\sigma_{\alpha,j}^{offline}$ associated to $m_{\alpha,j}^{offline}$. The mean signal to noise ratio of each ion (SNR_j) was calculated as:

$$SNR_j = \frac{\sum_\alpha \left(m_{\alpha,j}^{offline} / \sigma_{\alpha,j}^{offline}\right)}{N_{Filters}} \quad (3)$$

All ions with $SNR_j < 0.2$ were not considered, leaving 429 (out of 482) ions for PMF analysis. The error was increased for ions with $0.2 < SNR_j < 2$, by linearly scaling from a factor of 1 at $SNR_j = 2$ to a factor of 10 at $SNR_j = 0.2$.

A total organic carbon analyzer (TOC-L, Shimadzu) was used to quantify the water soluble organic carbon (WSOC) concentration of aqueous extracts of filter samples. Extracts were prepared following the same protocol as for the offline AMS analyses. The organic AMS spectra were then scaled to WSOA using Eq. (4).

$$m_{\alpha,j}^{offline,WSOA} = m_{\alpha,j}^{offline} \cdot \left(\frac{(OA/OC)_\alpha \cdot WSOC_\alpha}{\sum_j m_{\alpha,j}^{offline}}\right) \quad (4)$$

Here $(OA/OC)_\alpha$ denotes the mass ratio of organic aerosol to organic carbon, which is calculated on a spectrum-by-spectrum basis using the Igor analysis kit APES (Analytical Procedure for Elemental Separation, Aiken et al. (2008)). $WSOC_\alpha$ denotes the WSOC measurements. The corresponding $\sigma_{\alpha,j}^{offline,\ WSOA}$ values were calculated analogously by scaling $\sigma_{\alpha,j}^{offline}$ by the grouped terms in Eq. (4). The final WSOA spectra were obtained by subtracting from each filter spectrum the average spectrum of the WSOA field blank filters (FBs), and again the resulting uncertainty propagated to the error matrix, obtaining the final matrices of $m_{\alpha,j}^{PMF}$ and $\sigma_{\alpha,j}^{PMF}$ used for PMF input. This avoids introducing systematic biases (i.e., step changes in the input mass spectra) due to random deviations between individual FBs.

2.2.2. OC/EC and radiocarbon analyses

Organic and elemental carbon (OC, EC) were measured using an OC-EC Carbon Aerosol Analyzer (Sunset Laboratory Inc., USA) following the EUSAAR2 (European Supersites for Atmospheric Aerosol Research) protocol (Cavalli et al., 2010). Further details of the measurement methodology can be found in Samek et al. (2020a). In all, OC and EC were measured for 63 PM_1 filters and 62 PM_{10} filters (125 total, with the PM_{10} OC/EC measurement from 04.06.2018 missing), as well as for the 12 field blank filters. No EC was detected above detection limit in the field blank filters.

The fossil and modern fractions of the carbonaceous PM_1 were quantified by radiocarbon analyses. The one-step analysis protocol used to characterize the ^{14}C-TC of 62 PM_1 filters (including 8 field blank filters) involved the combustion of the sample under pure O_2 at 850 °C using an elemental analyzer (Salazar et al., 2015), and an online MIni radioCArbon DAting System (MICADAS) (Synal et al., 2007; Szidat et al., 2014) equipped with a gas ion source (Ruff et al., 2007) delivering $^{14}C/^{12}C$ isotopic ratio measurements. For the ^{14}C-TC measurements of 8 field blank filters, an OC-EC Carbon Aerosol Analyzer (Model 5 L, Sunset Laboratories Inc., USA) was coupled to the MICADAS (Agrios et al., 2015) instead of the elemental analyzer and the samples were combusted at 870 °C for 240 s under a stream of pure O_2. Radiocarbon measurements of field blank filters were performed only for TC since the field blank EC concentration was below detection limit. In addition, the modern EC fraction (fM_{EC}) was measured for a selected group of 20 PM_1 filter samples, distributed along the year but not matching any of the filters measured with the L-ToF-AMS (used to approximate fossil EC, see SI Section 7). The Swiss_4S protocol was used for all quantities measured with the OC-EC Carbon Aerosol Analyzer (Zhang et al., 2012). The modern fraction of OC (fM_{OC}) was calculated as difference between the modern TC and modern EC concentrations normalized to OC as:

$$fM_{OC} = \frac{TC \cdot fM_{TC} - TC_{FB} \cdot fM_{TC,FB} - EC \cdot fM_{EC}}{TC - TC_{FB} - EC}, \quad (5)$$

where fM_{TC} is the modern carbon fraction of TC, $fM_{TC,\ FB}$ the average modern carbon fraction of TC in the field blanks, and fM_{EC} the modern carbon fraction of EC. The OC_{fossil} is thus calculated as

$$OC_{fossil} = OC \cdot (1 - fM_{OC}) \quad (6)$$

2.2.3. Additional measurements

117 out of the 126 filters (59 PM_1, 58 PM_{10} filters, and 12 field blanks) were also analyzed for the concentrations of specific organic markers (levoglucosan, inositol, arabitol, mannosan, trehalose, mannitol, galactosan, glucose) using anion exchange chromatography with pulsed amperometric detection (HPAE-PAD). The samples were extracted in 3 mL of Milli-Q water, ultrasonicated for 30 min, and centrifuged at 4000 rpm for 10 min. The extracts were analyzed with a Dionex™ ICS3000 (Thermo Scientific™), equipped with a CarboPac™ MA1 column, utilizing a sodium hydroxide gradient of 480–650 mM and a flow rate of 0.4 mL min^{-1}, following the procedure explained in Iinuma et al. (2009).

The concentrations of selected elements (S, K, Ca, Ti, Mn, Fe, Cu, Zn, Br) were determined by energy dispersive X-ray fluorescence (XRF, details in Samek et al. (2020b)) for 46 filters from each size fraction (only for filters collected from April onwards). In brief, the XRF instrument was equipped with a 2 kW molybdenum tube as X-ray source, cooled by water. The excited X-rays were detected by a silicon-drift detector (SDD, KETEK) with an active surface of 70 mm^2, collimated up to 50 mm^2 and beryllium window with a thickness of 12.5 μm. The samples were placed on the eight-position sample changer holder (platter) with dedicated holders, which guarantees a constant measurement geometry. It should be noted that for a given type of sample (standard sample, air pollutant sample or pellets) the appropriate type of handle has been prepared. The platter is driven by a stepper motor. The created program in the LabVIEW environment enabled the automatic acquisition of X-ray spectra and the change of the

samples. The measurement time for each sample was 2400 s. The tube worked at a maximum voltage of 55 kV and a maximum current of 30 mA. These measurements were used as aid in identifying the OA sources through correlation analysis of the time series.

An aerosol speciation chemical monitor (ACSM, Aerodyne) measured non-refractory PM_1 online at the site during part of the filter collection campaign (8 January 2018 until 10 April 2019) (Tobler et al., 2021). The sampling method and operating details described by Ng et al. (2011b) were followed. The data were analyzed using ACSM Local 1.6.1.3 (Aerodyne Research Inc.) in Igor 6.37 (WaveMetrics, Inc.). The concentrations of NH_4, NO_3, SO_4, Cl, and OA, as well as the OA source apportionment results were used in support of the (offline) L-ToF-AMS-measured OA source apportionment.

2.3. Source apportionment techniques

This section provides brief explanations on the main algorithms and tools that were utilized to quantify the PM_1 and PM_{10} WSOA sources based on the mass spectral fingerprints provided by the L-ToF-AMS.

2.3.1. Positive matrix factorization

Source apportionment of WSOA was performed using positive matrix factorization (PMF), implemented with the Source Finder (SoFi, Datalystica) software package coupled to the multilinear engine-2 (ME-2) (Canonaco et al., 2013; Canonaco et al., 2021; Paatero, 1999). PMF is a bilinear receptor model with non-negativity constraints. PMF decomposes a matrix $m_{\alpha,j}^{PMF}$ (in this case, α being the time/filter index, j being the organic fragment ion index), into a user-selected number of target factors p. Each factor k' is characterized by the two vectors $g_{\alpha,k'}$, which represents the factor's concentration time series, and $f_{k',j}$, which represents the factor's chemical composition, and is obtained by solving the equation system

$$m_{\alpha,j}^{PMF} = \Sigma_{k=1}^{p} g_{\alpha,k} f_{k,j} + e_{\alpha,j}, \tag{7}$$

where $e_{\alpha,j}$ represents the residual of the model. PMF/ME-2 minimizes the quantity Q, defined as the sum of the squared uncertainty-weighted model residuals ($e_{\alpha,j}/\sigma_{\alpha,j}^{PMF}$), which were discussed in Section 2.2.1:

$$Q = \sum_{\alpha,j} \left(\frac{e_{\alpha,j}}{\sigma_{\alpha,j}^{PMF}} \right)^2 \tag{8}$$

Optimization continues until a pre-set number of iterations fail to yield a further decrease in Q (i.e., convergence) or the maximum iteration count is reached (non-convergence).

SoFi also allows users to access the constraint capabilities of ME-2. It gives the user the capability to constrain any of the factor profiles in $f_{k,j}$ with an externally determined profile f_j' and a tolerated relative deviation from the anchor defined by the parameter a (commonly referred to as the a value). It is implemented such that a constrained factor profile k' is limited by

$$f_{k',j}^{max,min} = f_j' \pm a_{k'} \cdot f_j' \tag{9}$$

Post-PMF renormalization of the solution profile f_{sol} can result in values that are slightly higher than $f_{k_1,j}^{max}$ or lower than $f_{k_1,j}^{min}$. Reference profiles were constructed for HOA (high resolution, HR: Mohr et al. (2012), unit mass resolution, UMR: Ng et al. (2011b)) and two for CCOA (HR_1: Elser et al. (2016), HR_2: Hu et al. (2013), UMR: Tobler et al. (2021)). In agreement with previous successful offline AMS source apportionment analysis quantifying HOA, the reference profiles used here for HOA and CCOA refer to total OA of the respective source. Nevertheless, recent work suggests that offline AMS source apportionment analyses might profit from creating reference profile libraries specific to the water-soluble fraction (Xu et al., 2020). Different kinds of combinations were considered to determine the optimal PMF solution (see SI Section 1 for details on the constrained factor profiles).

2.3.2. Bootstrapping

The uncertainty arising from the PMF analysis was assessed by bootstrapping the inputs for PMF (100 runs). Pearson correlations with the time series of the factors of the preliminary solution were used to sort the factors. The solutions to 19 PMF runs were excluded from the final analysis because the resolved BBOA factor's time series did not correlate with the one from the preliminary PMF solution. More details can be found in Table S1 and Fig. S10.

3. Results and discussion

3.1. WSOA sources

Here we identify and quantify the water-soluble (WS) fraction of OA sources. Both unconstrained and constrained PMF solutions with 6 to 8 factors were evaluated (see SI Section 2, Figs. S1, S2, S3, S4). Solutions with 5 factors were also considered, but they were discarded because all factors in the 6-factor solution were interpretable. Unconstrained solutions with 7 and more factors were discarded due to non-physical separation of the factors, evident from the time series and the Pearson correlation with ancillary data. The unconstrained 6-factor PMF solution was considered optimal and is shown here because it presented the best features among all considered PMF solutions, that is, the PM_1 time series of each factor was not inconsistently lower than the corresponding PM_{10} time series, the Pearson correlations showed reasonable values between the factors' time series and ancillary data, and mixing among factors was minimal (see SI Section 3). The analysis yielded three primary factors (primary biological OA (WS-PBOA), coarse OA linked to dust resuspension (WS-CoarseOA), and biomass burning OA (WS-BBOA)), as well as three secondary factors (winter oxygenated OA (WS-WOOA), summer oxygenated OA (WS-SOOA), and background oxygenated OA (WS-BkgOOA)). Fig. 1 displays the chemical composition (factor profiles) of the 6 WSOA factors. Fig. 2 displays the WSOA concentration time series of the sources, for PM_1 (blue lines) and PM_{10} (red lines), as well as the Pearson correlations (R_{Pr}) with a relevant tracer for WS-WOOA, WS-BBOA, and WS-CoarseOA, the Pearson correlation with two relevant tracers for WS-PBOA, and the Spearman correlation (R_{Sp}) with the temperature for WS-SOOA (since no linearity is expected). The correlations were always obtained by considering both size fractions simultaneously when available, except for Fig. 2b (WS-PBOA vs. mannitol + arabitol) where only PM_{10} was considered. The complete correlation table of each factor with the ancillary data is shown in Fig. S8. The scatter plot between the PM_{10} sum and PM_1 sum of all WSOA factor concentrations is shown in Fig. S5.

3.1.1. Primary WSOA

WS-BBOA is recognized by the typical profile and marker ions characteristic of biomass burning emissions (i.e., high contributions of the two marker fragment ions at m/z 60 ($C_2H_4O_2^+$) and 73 ($C_3H_5O_2^+$)) (Crippa et al., 2013; Ng et al., 2011a). WS-BBOA concentrations peak during the winter (from January to end of March) and show a temporal behavior correlating with levoglucosan (R_{Pr} = 0.72), an anhydrous sugar produced during wood burning (Simoneit et al., 1999). This factor is likely related to residential heating. Although WS-BBOA is expected to be mainly in PM_1, Fig. 2 shows somewhat higher concentrations in the PM_{10} fraction. However, since the $PM_{10} > PM_1$ observation for WS-BBOA mirrors a corresponding and clearly non-physical $PM_1 > PM_{10}$ observation for WS-WOOA (see Fig. S13), we conclude that these features likely result from imperfect separation of WS-BBOA and WS-WOOA.

WS-PBOA is predominantly observed in the coarse fraction (slope from linear fit of WS-PBOA(PM_{10}) vs. WS-PBOA(PM_1) = 3.2 ± 0.3 in spring and summer) and shows a clear enhancement in concentration during spring and summer with respect to winter. WS-PBOA correlates with markers of primary biological material such as mannitol (R_{Pr} = 0.75) and arabitol (R_{Pr} = 0.69), further supporting the identification of this factor (Bauer et al., 2008; Bozzetti et al., 2017a; Samaké et al., 2019a; Samaké et al., 2019b; Vlachou et al., 2019) (Figs. 2b–c, S7, S8). It is also the factor profile

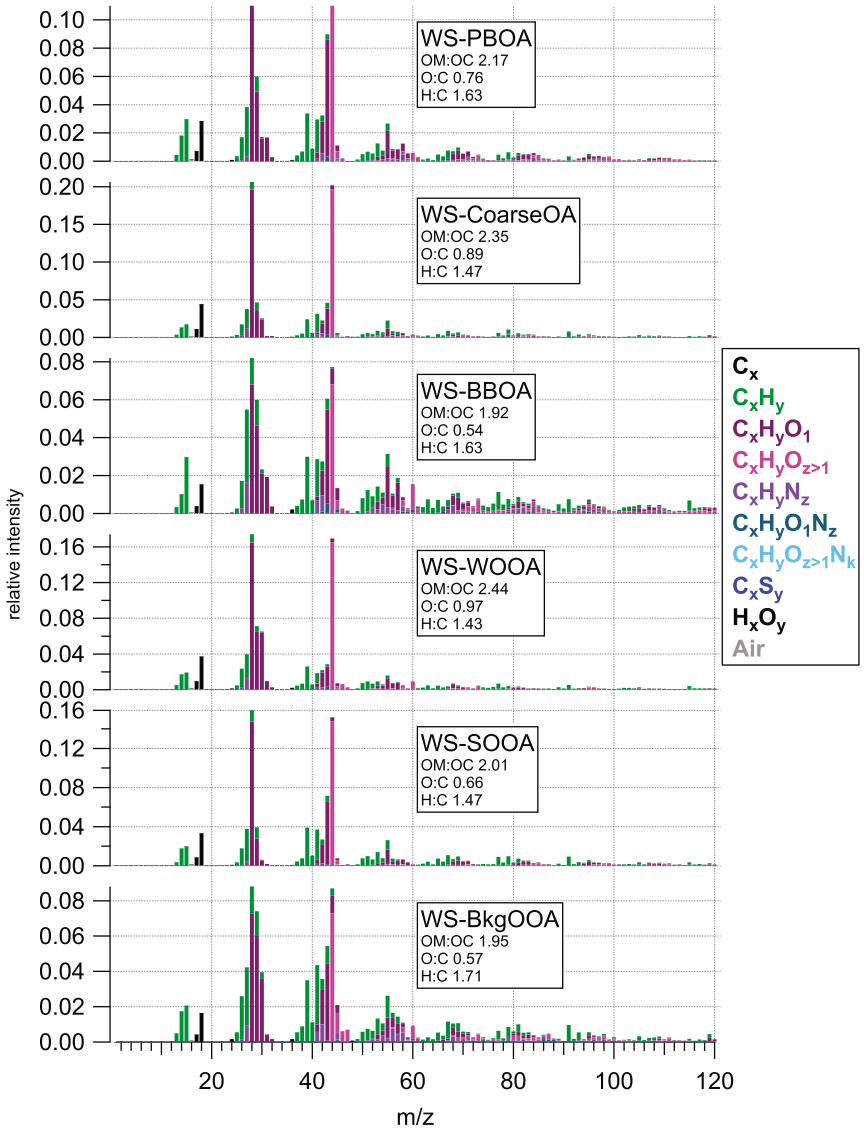

Fig. 1. Profiles of the 6 water-soluble OA factors.

with the highest ratio of $fC_2H_5O_2^+$ to $fC_2H_4O_2^+$ (ratio of 0.46; WS-CoarseOA with 0.4, no other factor is higher than 0.23), and it contains substantial amounts of nitrogen-containing compounds, in line with previously separated PBOA (Bozzetti et al., 2016) (see Fig. S7).

The WS-CoarseOA is believed to be related to mechanically generated resuspended material producing mainly particles larger than 1 μm, though with a tail of the size distribution contributing to PM_1. It has a large fraction of its mass in the coarse size fraction (slope of linear fit for WS-CoarseOA (PM_{10}) vs. WS-CoarseOA(PM_1) = 4 ± 1), is highly oxygenated (OA:OC = 2.35, O:C = 0.89), and correlates with Ca^{2+} (R_{Pr} = 0.77) (Lee and Pacyna, 1999). The high degree of oxygenation of WS-CoarseOA could at least in part be related to the detection of soluble carbonates which fragment to CO_2^+ in the AMS (Bozzetti et al., 2016).

3.1.2. Secondary WSOA

The secondary WSOA was apportioned to three factors (WS-WOOA, WS-SOOA, WS-BkgOOA) with distinctly different characteristics, as can be seen in Fig. 1 and Fig. 2. The resolved characteristics including seasonality and chemical profiles are in line with previous studies (Daellenbach et al., 2016; Daellenbach et al., 2017; Vlachou et al., 2018; Vlachou et al., 2019).

WS-WOOA is highly oxygenated (OA:OC = 2.44, O:C = 0.97, fCO_2^+ = 0.16) and exhibits high concentrations during the winter period while remaining near zero in the warmer seasons. WS-WOOA correlates with secondary inorganic constituents (R_{Pr} = 0.91 with NH_4, 0.88 with NO_3, and 0.76 with SO_4), indicating a prominent contribution of anthropogenic emissions to this factor, most likely coming from residential heating since no industrial fossil OC was detected during summer (Fig. 3c).

WS-SOOA is also highly oxygenated, yet less so than WS-WOOA (OA:OC = 2.01, O:C = 0.66, fCO_2^+ = 0.15). The WS-SOOA concentration strongly increases during summer, correlating with the temperature (R_{Sp} = 0.74). This suggests biogenic VOC emissions as a plausible main source (Fig. S6) (Leaitch et al., 2011; Vlachou et al., 2018; Vlachou et al., 2019). Interestingly, non-zero SOOA is observed in winter, consistent with several other studies (Casotto et al., 2022; Daellenbach et al., 2017). A possible reason may be the emission of fragranced volatile chemical products (VCPs), i.e., anthropogenic including personal care and cleaning products, which have been shown to contribute substantially to monoterpene emissions also during winter (Coggon et al., 2021). Indeed, two SOA factors were found in Zurich during winter in EESI-TOF-MS data that were qualitatively similar to factors retrieved from PMF analysis from the same site during summer, when monoterpenes are the dominant SOA precursors (Qi et al., 2019). Other possible explanations include the oxidation of monoterpenes from early stage wood combustion and a mathematical artifact of the PMF algorithm resulting

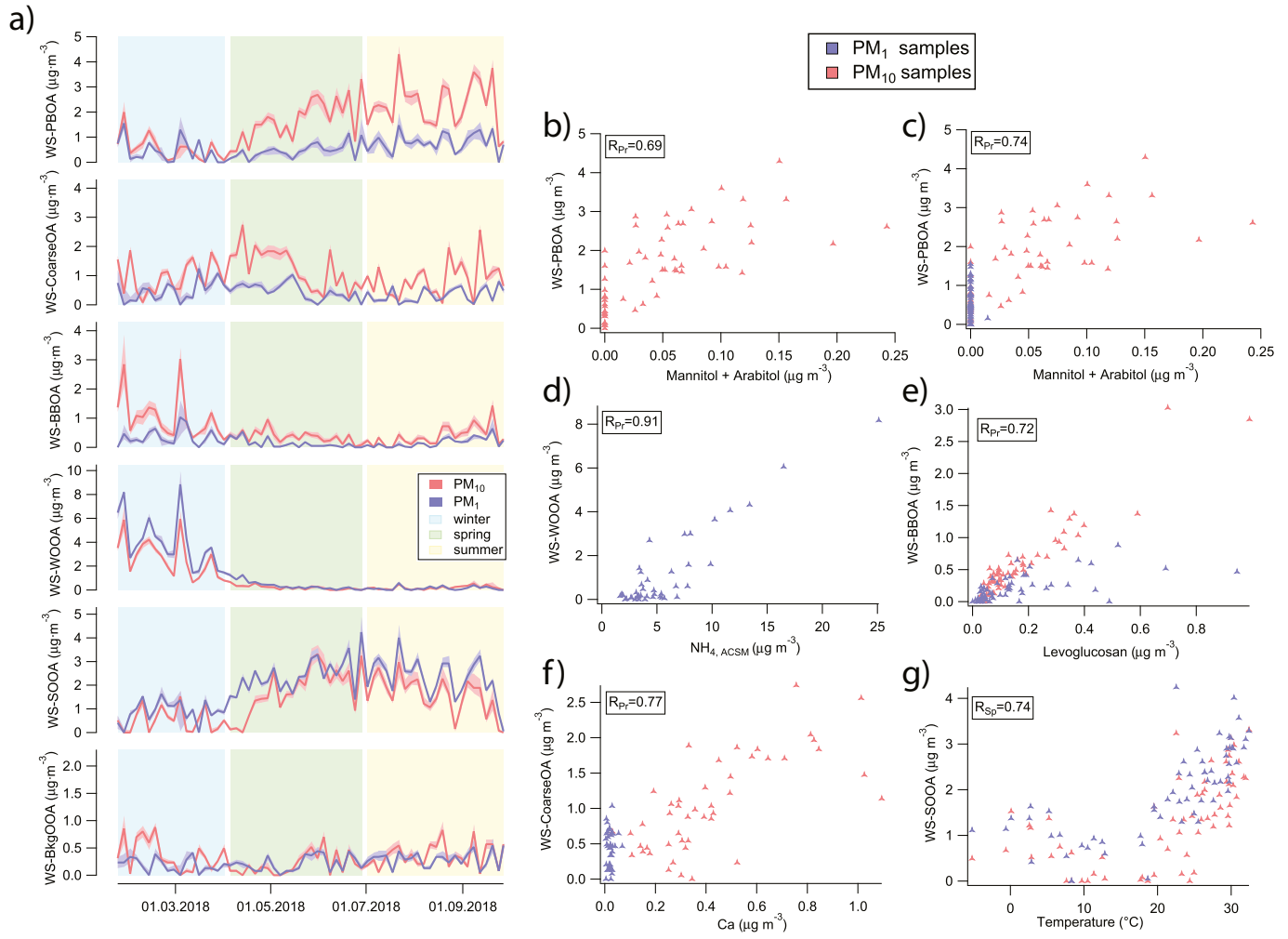

Fig. 2. (a) Time series of the average WSOA source apportioned factors from multiple bootstrapped inputs, with the median and the interquartile range displayed. The shaded uncertainties are bootstrap-derived, and the different seasons are displayed as background shades. (b) to (g) Scatter plots of the factor concentrations with the external measurements important for identification.

from its attempt to describe gradients in SOA composition using two static vectors (i.e., SOOA and WOOA mass spectra).

Both WS-WOOA and WS-SOOA are found predominantly in the PM_1 fraction of OA, with little to no presence in the coarse fraction (as discussed in Section 3.1.1, the higher PM_1 concentrations compared to the PM_{10} concentrations are considered to result from imperfect separation, e.g. WS-WOOA from WS-BBOA, Fig. S13). The WS-BkgOOA factor is highly oxygenated (OA:OC = 1.95, O:C = 0.57) and is believed to be a background secondary OA. Even though biomass burning marker fragment ions (*m/z* 60 and 73, i.e., $C_2H_4O_2^+$ and $C_3H_5O_2^+$) contribute considerably to WS-BkgOOA, we decided to keep WS-BkgOOA separated from primary biomass burning OA (WS-BBOA) because it does not correlate with any of the available ancillary data, including levoglucosan, and does not improve correlations with wood burning tracers when taken in sum with WS-BBOA. In any case, the concentration of WS-BkgOOA is very low compared to WS-BBOA, as well as to the other oxygenated factors, constituting 1 % of the PM_1 and 2 % of the PM_{10} OA in winter. As a result, the degree of possible factor mixing discussed above does not significantly affect the source apportionment.

3.2. Sources of water-insoluble OA

Fig. 3a–b show that the summer-time OC solubility in Krakow is largely consistent with previous analyses (e.g. Zurich spring-time and Paris summer- and winter-time WSOC/OC of 64–76 % (Daellenbach et al., 2016) as well as similar values for China at a rural site in the Guangzhou region reported by Xiao et al. (2011) and the US (rural site in Centreville, Alabama and urban site in Atlanta, Georgia by Xu et al. (2017a)) for both PM_1 (71 %) and PM_{10} (55 %) during summer. Fig. 3a–b also show that the winter-time OC solubility is substantially lower than the one detected at most other locations, and equally so for both PM_1 and PM_{10} (35 %), comparable to what was found during winter for the night-time SOA in Paris by Sciare et al. (2011) (41 %) and during spring for the low-volatility oxygenated OA (LV-OOA) factor in Helsinki by Timonen et al. (2013). The low OC solubility in winter highlights the large contribution of water-insoluble OC (e.g. hydrocarbons) that is not present in summer. The difference in proportions of factors between PM_1 and PM_{10} is due to the generation process of each source. For example, WS-PBOA (primary biological organic aerosol) is generated by mechanical processes, and probably likewise for WS-CoarseOA, leading to particles bigger than 1 µm being released into the atmosphere. Other factors are not generated by such mechanical processes, being, e.g., generated via combustion or condensation of secondary material, and therefore do not exhibit such PM_1 vs. PM_{10} differences.

Based on the assumption that all OC sources are represented by the WSOC source apportionment results, their recoveries (R_k, in essence water-solubility) can be empirically determined by fitting ambient OC as a function of the retrieved factors $\left(OC = \Sigma_k \frac{WSOC_k}{R_k}\right)$ (see SI Section 5). The retrieved factor concentrations ($WSOA_k$) are converted from OA to OC using the factor's (or field blank's) OA-to-OC ratios ($(OA/OC)_k$). For clarity, we refer to the factors that undergo this conversion without the WS- notation.

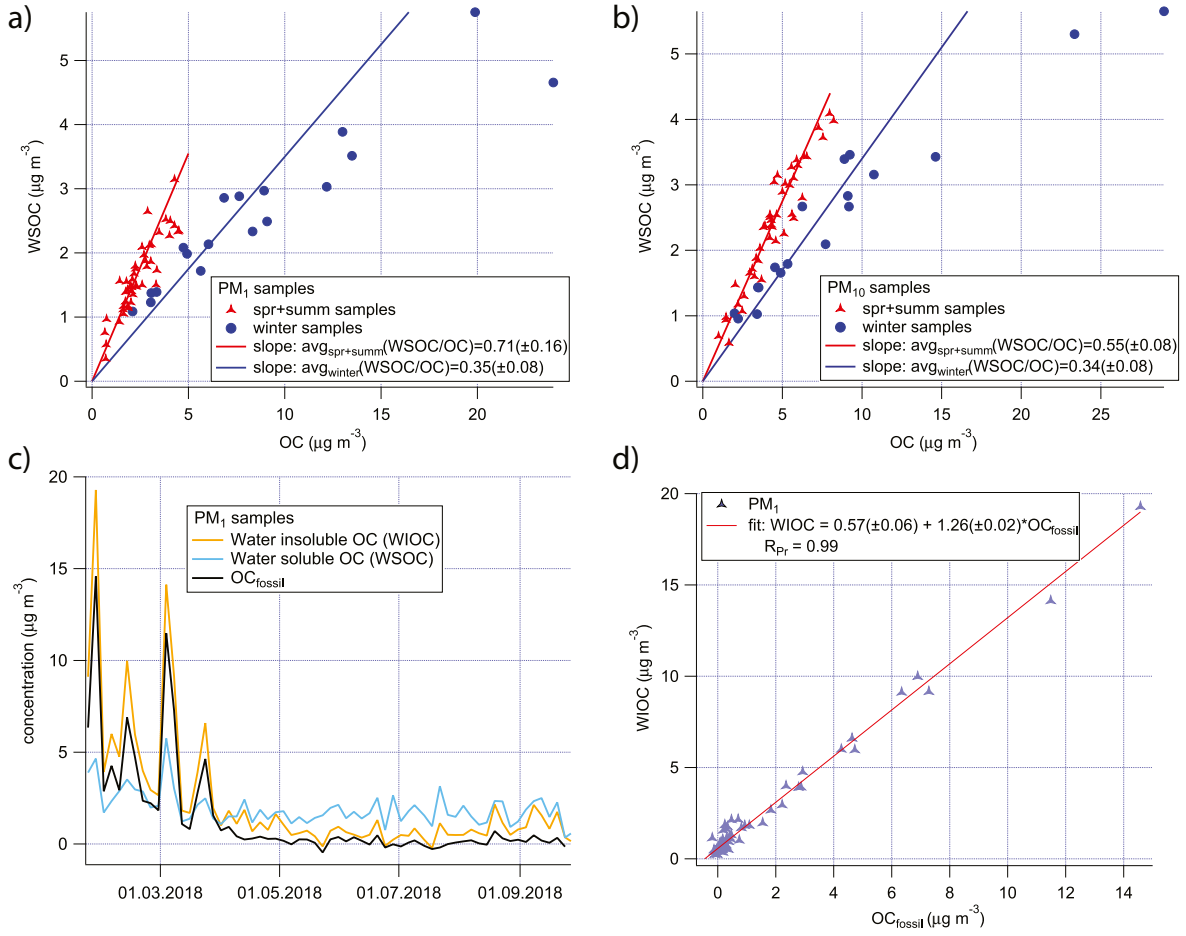

Fig. 3. (a) and (b) Scatter plots of WSOC vs OC for PM_1 and PM_{10}. The fits are divided into winter points and spring + summer points. (c) Time series of PM_1 concentration of the water soluble and insoluble OC together with the fossil OC. (d) Scatter plot of water insoluble OC versus fossil OC.

However, during winter the sum of the recovered OC sources is substantially lower than the measured OC (results in Table S2, Figs. S11, S12). In other words, the fit displays a large time-dependent residual (Fig. S12), not attributable to a systematic bias and thus not indicating a fit failure, but a missing OC source. This is despite the much lower than typical empirical winter-time OA source solubility values recovered (Fig. S5, Table S2); few studies have detected factors with such low solubility, for example in Estonia WOOA and BBOA were observed having similarly low solubilities (Vlachou et al., 2019), as well as for a similar factor (LV-OOA) in Helsinki, as already mentioned. The large time-dependent residual suggests that at least one wintertime OC source is not soluble — contradicting the initial assumption of the empirical recovery estimation. In fact, the total water-insoluble OC (WIOC) is highly correlated with fossil OC, as shown in Fig. 3. Therefore, it is highly likely that the missing OA source is related to fresh fossil fuel combustion. Given the seasonal cycle of fossil EC (estimated based on the EC_{fossil}/EC ratios of selected samples, see SI Section 7), we conclude that the missing source is fossil POA likely dominated by CCOA (see SI Sections 5 and 6). This is in line with a previous study identifying CCOA as a substantial contributor to winter-time OA in Krakow relying on in-situ ACSM analyses (Tobler et al., 2021).

In the following, we estimate the concentration of the missing CCOA source by OC mass balance using

$$\mathrm{CCOC} = \mathrm{OC} - \sum_{k=1,\ldots,6} \frac{WSOA_k}{R_k \cdot \left(\frac{\mathrm{OA}}{\mathrm{OC}}\right)_k}, \tag{10}$$

and assuming $(\mathrm{OA/OC})_{\mathrm{CCOA}} = 1.37$ (obtained from the CCOA factor separated in China by Elser et al. (2016)). The water-soluble OA source concentration time series ($WSOA_k$) and their OA/OC ratios are given by the PMF analysis, while the OC concentration is measured independently.

The most uncertain parameters in estimating CCOC are the recoveries of the WSOA sources, even though they were determined for similar sources at other locations previously. Here we determined the recoveries of the WSOA sources making the following assumptions.

1. The missing source is absent during summer, since during that period there is a negligible fossil OC concentration and the empirical recoveries do not show incongruences (Figs. S12, S14, S15). Therefore, the recovery-corrected factors need to explain summer-time OC without a bias, and the recoveries of the summer-time WSOA sources can be determined independently, since the winter-time WSOA sources (WS-WOOA, WS-CCOA) have negligible summer-time concentrations.
2. Only the winter-time WSOA sources include fossil OC (Figs. S14, S15), as implied by the factor definitions in Section 3.1. BBOA was considered to be completely non-fossil.
3. The missing OC source is related to fossil fuel combustion and therefore is assumed to be completely fossil-derived. Consequently, the fossil fraction of CCOC is assumed to be 1.

This leads to the additional mass balance equation for $\mathrm{OC_{fossil}}$

$$\mathrm{OC_{fossil}} = \mathrm{ffWOOC} \cdot \mathrm{WOOC} + \mathrm{ffCCOC} \cdot \mathrm{CCOC}, \tag{11}$$

in which ffWOOA and ffCCOC are the fossil fractions of WOOC and CCOC, and ffCCOC is assumed to be 1. We base the initial guess of source-specific OA recoveries on literature where available ($R_{\mathrm{PBOA}} = 0.41 \pm 0.01$, $R_{\mathrm{SOOA}} = 0.84 \pm 0.07$, $R_{\mathrm{BBOA}} = 0.61 \pm 0.02$ from Vlachou

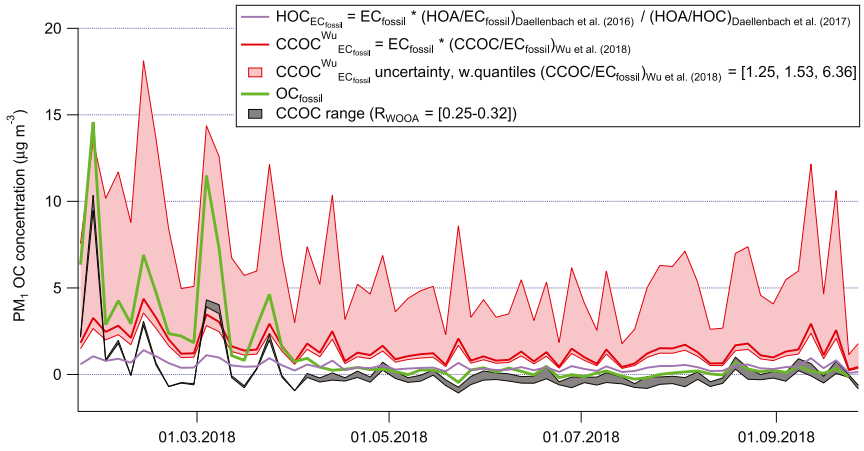

Fig. 4. Comparison between the time series of CCOC and the fossil OC, as well as the HOC and CCOC estimated assuming all EC is produced by liquid fuel combustion or coal combustion, respectively. Values for the estimates were obtained from different sources (Daellenbach et al., 2016; Daellenbach et al., 2017; Wu et al., 2018). The uncertainty of $CCOC^{Wu}$ was estimated by weighted quantiles.

et al. (2018)) and fix to 1 the recoveries for CoarseOA and BkgOOA based on the results obtained assuming that all OA sources are resolved (see SI Section 5). First, the recoveries of all but the winter-time factors are optimized to fit summer-time OC. Second, the unknown WOOA recovery is determined based on the winter-time data (results in Table S3) by using the constraint of ffCCOC = 1.

We find solubilities of SOOA and PBOA that are consistent with literature values at $1.00^{+0.00}_{-0.03}$ for SOOA and at 0.43 ± 0.02 for PBOA. The solubility of WOOA ($R_{WOOA} = 0.29^{+0.03}_{-0.04}$) is consistent with the one found in Estonia (see SI Section 6 for other OA sources). This is lower than for example in Switzerland, where a large fraction of WOOA is non-fossil and thought to originate from residential heating emissions dominated by wood combustion (Daellenbach et al., 2017; Daellenbach et al., 2020). In contrast, WOOA in Krakow contains a higher fraction of fossil carbon (ffWOOC = $0.48^{+0.01}_{-0.03}$) highlighting a prominent contribution of fossil fuel emissions, which are plausibly derived from coal combustion. This suggests that coal SOA is less water-soluble than wood burning SOA. The accuracy of the results was tested by simultaneously introducing an opposite bias of 5 % to the $WSOC_k$ and the OC in Eq. (10). The test showed no significant change in the results (Figs. S16a, S17, S18, and S19). Sensitivity tests assessing the impact of the imperfect separation between WS-BBOA and WS-WOOA show that it does not affect the OA source apportionment, the factors' water-solubility, or the fossil fraction of WOOA (Figs. S21, S22).

In Fig. 4, the CCOC concentration time series is compared to tracer-based concentration estimates of primary traffic exhaust and coal combustion, relying on the assumption that fossil EC is dominated by only one of them ($HOC_{EC_{fossil}}$, $CCOC_{EC_{fossil}}$) (see SI Section 7 for details). It is clear that while the estimate of liquid primary fossil fuel emissions ($HOC_{EC\text{-}fossil}$) cannot explain the missing OA source (CCOC) during the winter, the estimates of fresh residential coal combustion emissions ($CCOC^{Wu}_{EC\text{-}fossil}$) could account for the winter-time CCOC concentration (Wu et al., 2018). Nevertheless, HOC could contribute to CCOC as estimated here.

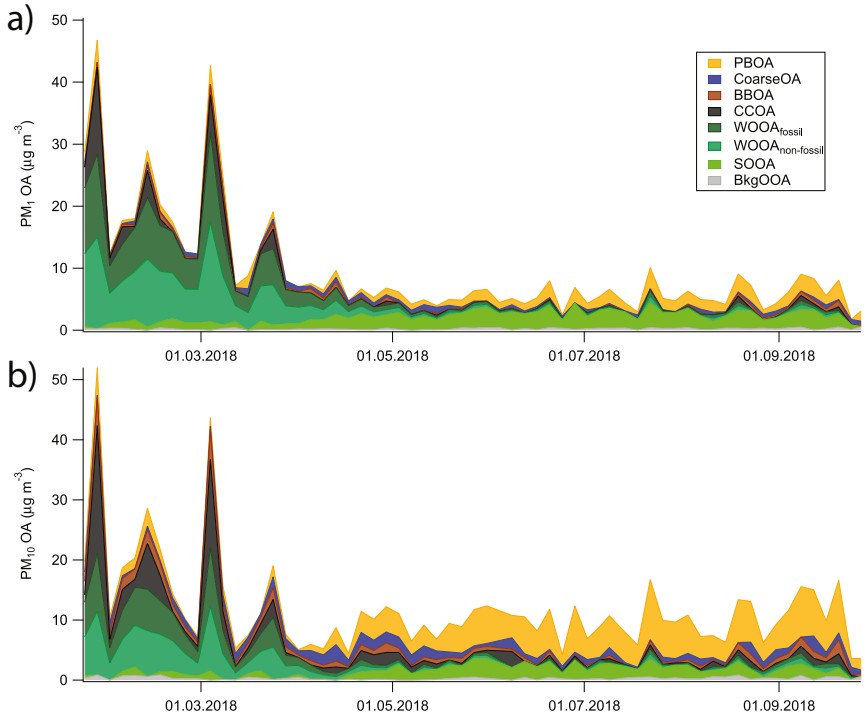

Fig. 5. Stacked OA source concentration time series for PM_1 (a) and PM_{10} (b). Only non-negative values of CCOA are displayed.

3.3. Source contributions to OA

This section summarizes the average concentration for each OA factor derived in the previous sections, categorized by season and size fraction. Fig. 5 shows the recovery-corrected stacked OA time series of PM_1 and PM_{10} of each source (corresponding stacked OC concentrations in Fig. S20). Fig. 6 displays the fractional contributions to OA of each factor by season and by concentration range. Table 1 summarizes the seasonal average concentrations for each factor, considering also the negative recovered values of CCOA.

PM_1 and PM_{10} OA concentrations exhibit a clear seasonality with maximum concentrations observed during winter (Fig. 5). In addition, the main OA sources vary substantially between seasons (Fig. 5). During summer, SOOA, which is related to the oxidation of biogenic VOC emissions (supported by the missing detection of fossil OC during summer), is the largest contributor to PM_1 OA (45 %). For PM_{10}, the largest contributors are PBOA (54 %) and SOOA (16 %). The OA sources dominating during summer are largely negligible during winter. Nevertheless, SOA contributes most to OA (77 % in PM_1 and 57 % in PM_{10}) during winter. Winter-time SOA has a much higher fossil fraction (44 %) than during summer (8 %) with the largest contributor being WOOA (34 % of OA, 48 % of fossil OA). The increase in WOOA is consistent with the increase in POA concentrations. Emissions from residential heating dominate winter-time POA

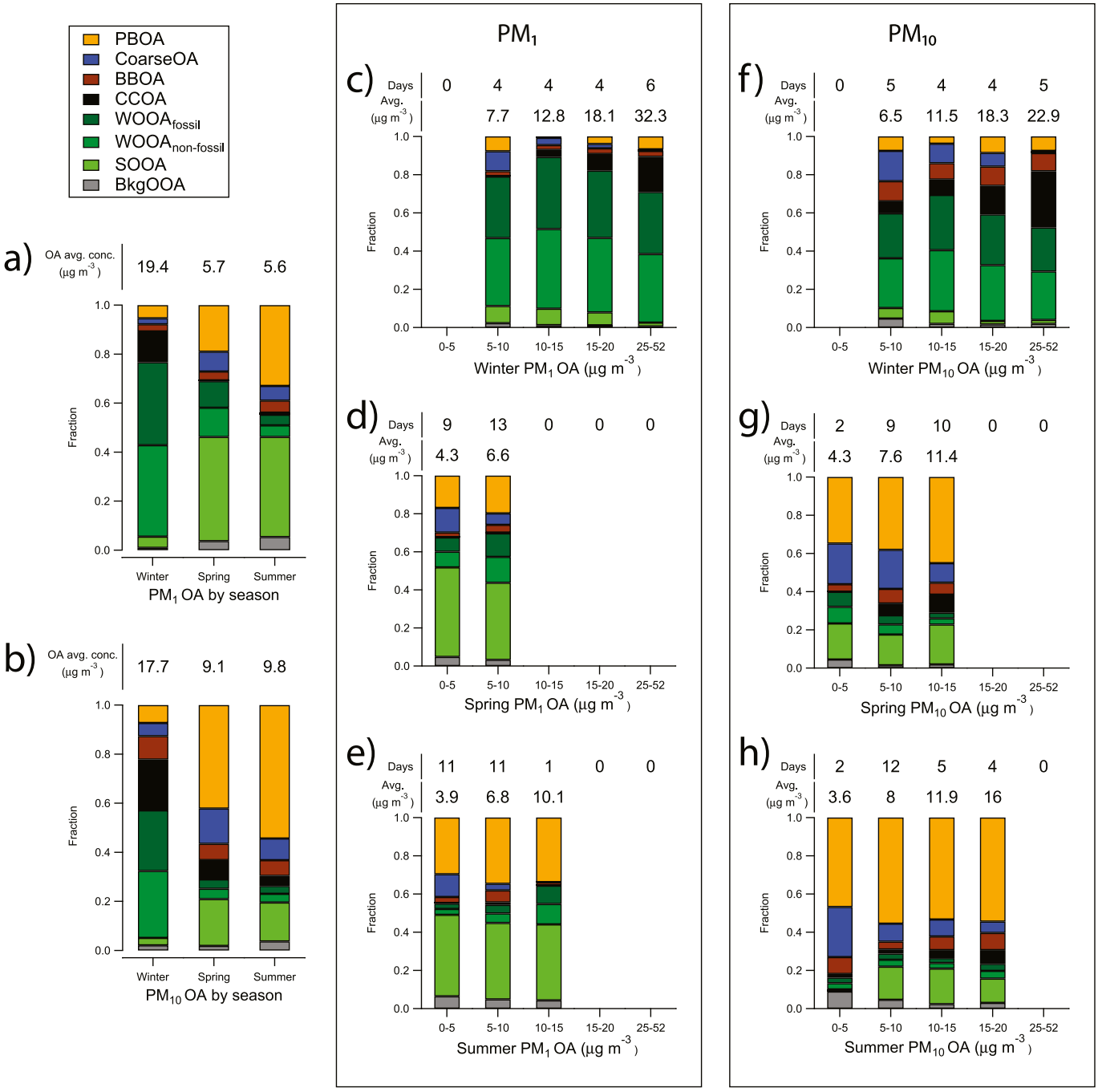

Fig. 6. (a) and (b) Stacked fractions of OA factors by season for PM_1 and PM_{10}, respectively. (c) to (e) Stacked fractions of PM_1 OA factors binned by concentration for the individual seasons, displaying also the number of days falling inside each concentration range, as well as the corresponding average concentration for each concentration range. (f) to (h) same as plots (c) to (e) but for the PM_{10} size fraction. Only non-negative concentrations of recovered CCOA were considered. Days are associated to winter from 23 Jan to 1 Apr, to spring from 5 Apr to 28 Jun, and to summer from 2 Jul to 27 Sept.

Table 1
Average concentration values for each OA source, separated for PM size fraction and season (uncertainties referring to the error of the average). Values in parentheses refer to the OA fraction relative to the specific season. Here, CCOA negative values are considered.

	PM_1		
	Winter ($\mu g\ m^{-3}$) (% of OA)	Spring ($\mu g\ m^{-3}$) (% of OA)	Summer ($\mu g\ m^{-3}$) (% of OA)
PBOA	1.0 ± 0.5 (5.5 ± 2.7 %)	1.1 ± 0.5 (20.0 ± 9.0 %)	1.8 ± 0.8 (34.7 ± 14.3 %)
CoarseOA	0.5 ± 0.2 (2.5 ± 1.2 %)	0.5 ± 0.1 (8.5 ± 2.7 %)	0.3 ± 0.1 (6.3 ± 2.1 %)
BBOA	0.6 ± 0.4 (2.9 ± 2.4 %)	0.2 ± 0.1 (3.8 ± 1.9 %)	0.3 ± 0.2 (5.2 ± 3.1 %)
CCOA	2.1 ± 1.9 (11.5 ± 9.9 %)	−0.3 ± 0.7 (−5.0 ± 12.4 %)	−0.2 ± 0.8 (−4.3 ± 14.8 %)
$WOOA_{fossil}$	6.5 ± 0.8 (34.4 ± 4.3 %)	0.6 ± 0.2 (11.4 ± 2.8 %)	0.2 ± 0.1 (4.6 ± 2.5 %)
$WOOA_{nn\text{-}fos}$	7.2 ± 0.9 (38.0 ± 4.8 %)	0.7 ± 0.2 (12.6 ± 3.1 %)	0.3 ± 0.1 (5.0 ± 2.8 %)
SOOA	0.9 ± 0.3 (4.7 ± 1.5 %)	2.4 ± 0.3 (44.8 ± 5.0 %)	2.3 ± 0.3 (42.9 ± 6.2 %)
BkgOOA	0.2 ± 0.2 (1.0 ± 1.3 %)	0.2 ± 0.2 (3.9 ± 3.0 %)	0.3 ± 0.2 (5.6 ± 3.8 %)
	PM_{10}		
	Winter ($\mu g\ m^{-3}$) (% of OA)	Spring ($\mu g\ m^{-3}$) (% of OA)	Summer ($\mu g\ m^{-3}$) (% of OA)
PBOA	1.3 ± 0.5 (7.3 ± 3.1 %)	3.9 ± 0.9 (42.2 ± 9.5 %)	5.3 ± 1.1 (54.4 ± 11.5 %)
CoarseOA	0.9 ± 0.2 (5.4 ± 1.3 %)	1.3 ± 0.2 (14.4 ± 2.4 %)	0.9 ± 0.2 (8.8 ± 1.8 %)
BBOA	1.7 ± 0.6 (9.6 ± 3.6 %)	0.6 ± 0.3 (6.6 ± 3.3 %)	0.6 ± 0.4 (6.4 ± 3.6 %)
CCOA	3.7 ± 2.2 (20.7 ± 12.2 %)	0.7 ± 1.2 (7.9 ± 12.9 %)	0.4 ± 1.3 (4.1 ± 13.4 %)
$WOOA_{fossil}$	4.4 ± 0.9 (24.7 ± 5.3 %)	0.3 ± 0.2 (3.8 ± 2.3 %)	0.3 ± 0.2 (3.2 ± 2.3 %)
$WOOA_{nn\text{-}foss}$	4.8 ± 1.0 (27.3 ± 5.9 %)	0.4 ± 0.2 (4.2 ± 2.5 %)	0.3 ± 0.2 (3.5 ± 2.5 %)
SOOA	0.5 ± 0.2 (3.0 ± 1.4 %)	1.7 ± 0.4 (19.0 ± 4.3 %)	1.6 ± 0.5 (15.8 ± 5.3 %)
BkgOOA	0.4 ± 0.2 (2.1 ± 0.9 %)	0.2 ± 0.1 (1.9 ± 1.2 %)	0.4 ± 0.2 (3.7 ± 1.6 %)

(BBOA: 13 % of POA, CCOA: 51 % of POA). Overall, OA from fossil-fuel combustion contributes 46 % (12 % from CCOA and 34 % from $WOOA_{fossil}$) to total fine OA (summer-time fossil OC < 0.5 $\mu g\ m^{-3}$). In PM_{10}, mechanically generated coarse POA (PBOA: 54 %, CoarseOA: 9 %) plays an important role in addition to winter-time BBOA, and CCOA and peaks in spring and summer. The OA concentrations vary substantially more during winter than during summer (PM_{10} OA, winter: 9.8 ± 8.8 $\mu g\ m^{-3}$, summer: 3.9 ± 1.9 $\mu g\ m^{-3}$). During summer, no particular OA source is related to high OA concentration periods, while during winter increasing OA pollution levels are associated with an enhanced CCOA contribution (Fig. 6).

A comparison of the offline AMS source apportionment results to results from a collocated online PM_1 ACSM deployment is displayed in the supplementary information (SI Fig. 23). The analyses differ in that the offline AMS identifies contributions to PM_1 from mechanically-generated OA sources (PBOA, CoarseOA), while these sources are not detected by the online ACSM. Because these particles occur predominantly above 1 μm, their contribution to PM_1 represents only a tail of the size distribution and is likely dominated by particles that are only slightly smaller than the 1 μm cutoff. The absence of such factors in the ACSM is likely related to inefficient transmission of particles near the ~1 μm cutoff through the ACSM PM_1 inlet and lens (Peck et al., 2016; Xu et al., 2017b). A second difference is that the ACSM finds a larger POA-to-SOA ratio (50 %) than in this study (28 % in PM_1), in particular in winter (Tobler et al., 2021), highlighting uncertainties in separating POA from SOA during polluted winter-time conditions as observed also in previous studies (Chen et al., 2021).

4. Conclusions

In this study, we examined the OA sources in Krakow, Poland, a European pollution hotspot, prior to the implementation of a city-wide ban on the use of solid fuels for residential heating. We find that winter and summer OA were dominated by different sources. During winter, secondary OA (SOA) was the main contributor to OA (78 % in PM_1, 57 % in PM_{10}), composed of approximately equal parts of fossil and non-fossil material. WOOA was related to anthropogenic emissions, likely from residential heating, and was the major contributor to OA (72 % of PM_1, 52 % of PM_{10}). In addition, fresh solid fuel combustion emissions from residential heating contribute to OA during winter (CCOA: 12 %, BBOA: 2.9 %). While BBOA contributed substantially to WSOA, the water-soluble fraction of coal combustion OA (COOA) was too small to be quantified in this study, suggesting that CCOA was highly water-insoluble. This is consistent with WOOA being fairly insoluble (R_{WOOA} = 0.29). In contrast, spring and summer were dominated by biogenic sources (non-fossil), i.e., fine biogenic secondary oxygenated OA (SOOA: 35 % in PM_1) and coarse primary biological OA (PBOA: 54 % in PM_{10}). As mentioned, this study characterizes the situation before residential heating using solid fuel combustion appliances was banned in Krakow. In order to determine the effect of the implemented policy, future studies are needed to quantify the OA sources in the coming years. Such research overall will allow determining on which spatial scale mitigation policies are required to have an impact on local air quality.

CRediT authorship contribution statement

RC: investigation, methodology, software, formal analysis, data curation, writing – original draft, visualization.

AS: investigation, formal analysis, validation, resources, funding acquisition.

MR: investigation, formal analysis, writing- review and editing.

JS: investigation, formal analysis, writing- review and editing.

AT: investigation, filter collection.

DB: investigation.

HL: investigation.

MIM: formal analysis.

GS: software, formal analysis.

TC: methodology.

FC: methodology.

LS: formal analysis, validation, methodology, resources.

AR: investigation, formal analysis, methodology.

IEH: project administration.

AKG: resources.

UB: validation, supervision.

JN: conceptualization, resources.

SS: resources.

KS: resources, project administration, investigation, validation, funding acquisition.

JGS: methodology, validation, supervision, writing – original draft.

ASHP: conceptualization, resources, project administration, funding acquisition, supervision, writing – original draft.

KRD: investigation, methodology, supervision, conceptualization, validation, writing – original draft.

Funding information

This project was supported by the Swiss National Science Foundation (BSSGI0_155846 and Ambizione grant PZPGP2_201992), as well as the EU Horizon 2020 Framework Programme via the ERAPLANET project SMURBS (grant agreement no. 689443). Research was also supported by Research Subsidies AGH 16.16.210.476 and AGH 16.16.220.842. Contribution of AS and KS was supported by the Polish National Science Centre (grant no. 2019/33/N/ST10/02925) and by the EU Project POWR.03.02.00-00-I004/16.

Data availability

The input data to the PMF and data in the figures are available in the Zenodo repository https://doi.org/10.5281/zenodo.7071648.

Declaration of competing interest

Francesco Canonaco and Anna Tobler work for Datalystica Ltd., which provides the SoFi software used in this paper. Otherwise, the authors declare that they have no known competing financial interests or personal relationships that could have appeared to influence the work reported in this paper.

Acknowledgments

We thank Valya Dzhambazova and Abdelaziz Boudellioua for helping with filter management, sample preparation, and fossil carbon fraction measurements, Stamatios Giannoukos for helping with the measurements during weekends, and Jens Top and Marion Lara Audrey Gosselin for helping with the TOC analyzer measurements.

Appendix A. Supplementary data

Supplementary data to this article can be found online at https://doi.org/10.1016/j.scitotenv.2022.158655.

References

Agrios, K., Salazar, G., Zhang, Y.-L., Uglietti, C., Battaglia, M., Luginbühl, M., et al., 2015. Online coupling of pure O_2 thermo-optical methods – ^{14}C AMS for source apportionment of carbonaceous aerosols. Nucl. Instrum. Methods Phys. Res., Sect. B 361, 288–293.

Aiken, A.C., DeCarlo, P.F., Kroll, J.H., Worsnop, D.R., Huffman, J.A., Docherty, K.S., et al., 2008. O/C and OM/OC ratios of primary, secondary, and ambient organic aerosols with high-resolution time-of-flight aerosol mass spectrometry. Environ. Sci. Technol. 42, 4478–4485.

Almeida, S.M., Manousakas, M., Diapouli, E., Kertesz, Z., Samek, L., Hristova, E., et al., 2020. Ambient particulate matter source apportionment using receptor modelling in European and Central Asia urban areas. Environ. Pollut. 266, 115199.

Barmpadimos, I., Keller, J., Oderbolz, D., Hueglin, C., Prévôt, A.S.H., 2012. One decade of parallel fine (PM2.5) and coarse (PM10–PM2.5) particulate matter measurements in Europe: trends and variability. Atmos. Chem. Phys. 12, 3189–3203.

Bauer, H., Claeys, M., Vermeylen, R., Schueller, E., Weinke, G., Berger, A., et al., 2008. Arabitol and mannitol as tracers for the quantification of airborne fungal spores. Atmos. Environ. 42, 588–593.

Beloconi, A., Vounatsou, P., 2021. Substantial reduction in particulate matter air pollution across Europe during 2006–2019: a spatiotemporal modeling analysis. Environ. Sci. Technol. 55, 15505–15518.

Bibler, C.J., Marshall, J.S., Pilcher, R.C., 1998. Status of worldwide coal mine methane emissions and use. Int. J. Coal Geol. 35, 283–310.

Błaszczak, B., Mathews, B., 2020. Characteristics of carbonaceous matter in aerosol from selected urban and rural areas of southern Poland. Atmosphere 11 (7), 687.

Błaszczak, B., Zioła, N., Mathews, B., Klejnowski, K., Słaby, K., 2020. The role of PM2.5 chemical composition and meteorology during high pollution periods at a suburban background station in southern Poland. Aerosol Air Qual. Res. 20, 2433–2447.

Bozzetti, C., Daellenbach, K.R., Hueglin, C., Fermo, P., Sciare, J., Kasper-Giebl, A., et al., 2016. Size-resolved identification, characterization, and quantification of primary biological organic aerosol at a European rural site. Environ. Sci. Technol. 50, 3425–3434.

Bozzetti, C., El Haddad, I., Salameh, D., Daellenbach, K.R., Fermo, P., Gonzalez, R., et al., 2017a. Organic aerosol source apportionment by offline-AMS over a full year in Marseille. Atmos. Chem. Phys. 17, 8247–8268.

Bozzetti, C., Sosedova, Y., Xiao, M., Daellenbach, K.R., Ulevicius, V., Dudoitis, V., et al., 2017b. Argon offline-AMS source apportionment of organic aerosol over yearly cycles for an urban, rural, and marine site in northern Europe. Atmos. Chem. Phys. 17, 117–141.

Burnett, R., Chen, H., Szyszkowicz, M., Fann, N., Hubbell, B., Pope, C.A., et al., 2018. Global estimates of mortality associated with long-term exposure to outdoor fine particulate matter. Proc. Natl. Acad. Sci. 115, 9592.

Canonaco, F., Crippa, M., Slowik, J., Baltensperger, U., Prévôt, A., 2013. SoFi, an IGOR-based interface for the efficient use of the generalized multilinear engine (ME-2) for the source apportionment: ME-2 application to aerosol mass spectrometer data. Atmos. Meas. Tech. 6, 3649–3661.

Canonaco, F., Tobler, A., Chen, G., Sosedova, Y., Slowik, J.G., Bozzetti, C., et al., 2021. A new method for long-term source apportionment with time-dependent factor profiles and uncertainty assessment using SoFi pro: application to 1 year of organic aerosol data. Atmos. Meas. Tech. 14, 923–943.

Casotto, R., Cvitešić Kušan, A., Bhattu, D., Cui, T., Manousakas, M.I., Frka, S., et al., 2022. Chemical composition and sources of organic aerosol on the Adriatic coast in Croatia. Atmos. Environ. X 13, 100159.

Cavalli, F., Viana, M., Yttri, K.E., Genberg, J., Putaud, J.P., 2010. Toward a standardised thermal-optical protocol for measuring atmospheric organic and elemental carbon: the EUSAAR protocol. Atmos. Meas. Tech. 3, 79–89.

Chen, G., Sosedova, Y., Canonaco, F., Fröhlich, R., Tobler, A., Vlachou, A., et al., 2021. Time-dependent source apportionment of submicron organic aerosol for a rural site in an alpine valley using a rolling positive matrix factorisation (PMF) window. Atmos. Chem. Phys. 21, 15081–15101.

Choi, H., Melly, S., Spengler, J., 2015. Intraurban and longitudinal variability of classical pollutants in Kraków, Poland, 2000–2010. Int. J. Environ. Res. Public Health 12 (5), 4967–4991.

Coggon, M.M., Gkatzelis, G.I., McDonald, B.C., Gilman, J.B., Schwantes, R.H., Abuhassan, N., et al., 2021. Volatile chemical product emissions enhance ozone and modulate urban chemistry. Proc. Natl. Acad. Sci. 118, e2026653118.

Crippa, M., DeCarlo, P.F., Slowik, J.G., Mohr, C., Heringa, M.F., Chirico, R., et al., 2013. Wintertime aerosol chemical composition and source apportionment of the organic fraction in the metropolitan area of Paris. Atmos. Chem. Phys. 13, 961–981.

Daellenbach, K.R., Bozzetti, C., Křepelová, A., Canonaco, F., Wolf, R., Zotter, P., et al., 2016. Characterization and source apportionment of organic aerosol using offline aerosol mass spectrometry. Atmos. Meas. Tech. 9, 23–39.

Daellenbach, K.R., Stefenelli, G., Bozzetti, C., Vlachou, A., Fermo, P., Gonzalez, R., et al., 2017. Long-term chemical analysis and organic aerosol source apportionment at nine sites in Central Europe: source identification and uncertainty assessment. Atmos. Chem. Phys. 17, 13265–13282.

Daellenbach, K.R., Uzu, G., Jiang, J., Cassagnes, L.-E., Leni, Z., Vlachou, A., et al., 2020. Sources of particulate-matter air pollution and its oxidative potential in Europe. Nature 587, 414–419.

Elser, M., Huang, R.-J., Wolf, R., Slowik, J.G., Wang, Q., Canonaco, F., et al., 2016. New insights into PM2.5 chemical composition and sources in two major cities in China during extreme haze events using aerosol mass spectrometry. Atmos. Chem. Phys. 16, 3207–3225.

Fabiańska, M.J., Kozielska, B., Konieczyński, J., Kowalski, A., 2016. Sources of organic pollution in particulate matter and soil of silesian agglomeration (Poland): evidence from geochemical markers. Environ. Geochem. Health 38, 821–842.

Górka, M., Kosztowniak, E., Lewandowska, A.U., Widory, D., 2020. Carbon isotope compositions and TC/OC/EC levels in atmospheric PM10 from lower Silesia (SW Poland): spatial variations, seasonality, sources and implications. Atmos. Pollut. Res. 11, 1099–1114.

Górka, M., Rybicki, M., Simoneit, B.R.T., Marynowski, L., 2014. Determination of multiple organic matter sources in aerosol PM10 from Wrocław, Poland using molecular and stable carbon isotope compositions. Atmos. Environ. 89, 739–748.

Grant, D., Zelinka, D., Mitova, S., 2021. Reducing CO^2 emissions by targeting the world's hyper-polluting power plants. Environ. Res. Lett. 16, 094022.

Gruszecka-Kosowska, A., 2018. Assessment of the Kraków inhabitants' health risk caused by the exposure to inhalation of outdoor air contaminants. Stoch. Env. Res. Risk A 32, 485–499.

Hu, W.W., Hu, M., Yuan, B., Jimenez, J.L., Tang, Q., Peng, J.F., et al., 2013. Insights on organic aerosol aging and the influence of coal combustion at a regional receptor site of central eastern China. Atmos. Chem. Phys. 13, 10095–10112.

Iinuma, Y., Engling, G., Puxbaum, H., Herrmann, H., 2009. A highly resolved anion-exchange chromatographic method for determination of saccharidic tracers for biomass combustion and primary bio-particles in atmospheric aerosol. Atmos. Environ. 43, 1367–1371.

IPCC, 2014. Climate Change 2014: Synthesis Report. Contribution of Working Groups I, II and III to the Fifth Assessment Report of the Intergovernmental Panel on Climate Change. IPCC, Geneva, Switzerland, p. 151.

Jimenez, J.L., Canagaratna, M.R., Donahue, N.M., Prevot, A.S.H., Zhang, Q., Kroll, J.H., et al., 2009. Evolution of organic aerosols in the atmosphere. Science 326, 1525–1529.

Junninen, H., Mønster, J., Rey, M., Cancelinha, J., Douglas, K., Duane, M., et al., 2009. Quantifying the impact of residential heating on the urban air quality in a typical European coal combustion region. Environ. Sci. Technol. 43, 7964–7970.

Kiesewetter, G., Schoepp, W., Heyes, C., Amann, M., 2015. Modelling PM2.5 impact indicators in Europe: health effects and legal compliance. Environ. Model Softw. 74, 201–211.

Kristensson, A., Ausmeel, S., Pauraite, J., Eriksson, A., Ahlberg, E., Byčenkienė, S., et al., 2020. Source contributions to rural carbonaceous winter aerosol in north-eastern Poland. Atmosphere 11, 263.

Leaitch, W.R., Macdonald, A.M., Brickell, P.C., Liggio, J., Sjostedt, S.J., Vlasenko, A., et al., 2011. Temperature response of the submicron organic aerosol from temperate forests. Atmos. Environ. 45, 6696–6704.

Lee, D.S., Pacyna, J.M., 1999. An industrial emissions inventory of calcium for Europe. Atmos. Environ. 33, 1687–1697.

Mohr, C., DeCarlo, P.F., Heringa, M.F., Chirico, R., Slowik, J.G., Richter, R., et al., 2012. Identification and quantification of organic aerosol from cooking and other sources in Barcelona using aerosol mass spectrometer data. Atmos. Chem. Phys. 12, 1649–1665.

Ng, N.L., Canagaratna, M.R., Jimenez, J.L., Zhang, Q., Ulbrich, I.M., Worsnop, D.R., 2011a. Real-time methods for estimating organic component mass concentrations from aerosol mass spectrometer data. Environ. Sci. Technol. 45, 910–916.

Ng, N.L., Herndon, S.C., Trimborn, A., Canagaratna, M.R., Croteau, P., Onasch, T.B., et al., 2011b. An aerosol chemical speciation monitor (ACSM) for routine monitoring of the composition and mass concentrations of ambient aerosol. Aerosol Sci. Technol. 45, 780–794.

Paatero, P., 1999. The multilinear engine—a table-driven, least squares program for solving multilinear problems, including the n-way parallel factor analysis model. J. Comput. Graph. Stat. 8, 854–888.

Peck, J., Gonzalez, L.A., Williams, L.R., Xu, W., Croteau, P.L., Timko, M.T., et al., 2016. Development of an aerosol mass spectrometer lens system for PM2.5. Aerosol Sci. Technol. 50, 781–789.

Pieber, S.M., El Haddad, I., Slowik, J.G., Canagaratna, M.R., Jayne, J.T., Platt, S.M., et al., 2016. Inorganic salt interference on CO2+ in aerodyne AMS and ACSM organic aerosol composition studies. Environ. Sci. Technol. 50, 10494–10503.

Ruff, M., Wacker, L., Gäggeler, H.W., Suter, M., Synal, H.A., Szidat, S., 2007. A gas ion source for radiocarbon measurements at 200 kV. Radiocarbon 49, 307–314.

Salazar, G., Zhang, Y.L., Agrios, K., Szidat, S., 2015. Development of a method for fast and automatic radiocarbon measurement of aerosol samples by online coupling of an elemental analyzer with a MICADAS AMS. Nucl. Instrum. Methods Phys. Res., Sect. B 361, 163–167.

Samaké, A., Jaffrezo, J.L., Favez, O., Weber, S., Jacob, V., Albinet, A., et al., 2019a. Polyols and glucose particulate species as tracers of primary biogenic organic aerosols at 28 french sites. Atmos. Chem. Phys. 19, 3357–3374.

Samaké, A., Jaffrezo, J.L., Favez, O., Weber, S., Jacob, V., Canete, T., et al., 2019b. Arabitol, mannitol, and glucose as tracers of primary biogenic organic aerosol: the influence of environmental factors on ambient air concentrations and spatial distribution over France. Atmos. Chem. Phys. 19, 11013–11030.

Samek, L., Stegowski, Z., Styszko, K., Furman, L., Zimnoch, M., Skiba, A., et al., 2020a. Seasonal variations of chemical composition of PM2.5 fraction in the urban area of Krakow, Poland: PMF source attribution. Air Qual. Atmos. Health 13, 89–96.

Samek, L., Turek-Fijak, A., Skiba, A., Furman, P., Styszko, K., Furman, L., et al., 2020b. Complex characterization of fine fraction and source contribution to PM2.5 mass at an urban area in Central Europe. Atmosphere 11, 1085.

Sciare, J., d'Argouges, O., Sarda-Estève, R., Gaimoz, C., Dolgorouky, C., Bonnaire, N., et al., 2011. Large contribution of water-insoluble secondary organic aerosols in the region of Paris (France) during wintertime. J. Geophys. Res. Atmos. 116.

Simoneit, B.R.T., Schauer, J.J., Nolte, C.G., Oros, D.R., Elias, V.O., Fraser, M.P., et al., 1999. Levoglucosan, a tracer for cellulose in biomass burning and atmospheric particles. Atmos. Environ. 33, 173–182.

Stala-Szlugaj, K., 2018. The demand for hard coal for households in Poland and the anti-smog bill. Arch. Min. Sci. 63, 701–711.

Synal, H.-A., Stocker, M., Suter, M., 2007. MICADAS: a new compact radiocarbon AMS system. Nucl. Instrum. Methods Phys. Res., Sect. B 259, 7–13.

Szidat, S., Salazar, G.A., Vogel, E., Battaglia, M., Wacker, L., Synal, H.-A., et al., 2014. 14C analysis and sample preparation at the New Bern Laboratory for the analysis of radiocarbon with AMS (LARA). Radiocarbon 56, 561–566.

Szramowiat, K., Styszko, K., Kistler, M., Kasper-Giebl, A., Gołaś, J., 2016. Carbonaceous species in atmospheric aerosols from the Krakow area (Malopolska District): carbonaceous species dry deposition analysis. E3S Web Conf. 10.

Timonen, H., Carbone, S., Aurela, M., Saarnio, K., Saarikoski, S., Ng, N.L., et al., 2013. Characteristics, sources and water-solubility of ambient submicron organic aerosol in springtime in Helsinki, Finland. J. Aerosol Sci. 56, 61–77.

Tobler, A.K., Skiba, A., Canonaco, F., Močnik, G., Rai, P., Chen, G., et al., 2021. Characterization of NR-PM1 and source apportionment of organic aerosol in Krakow, Poland. Atmos. Chem. Phys. 21, 14893–14906.

Ulbrich, I.M., Canagaratna, M.R., Zhang, Q., Worsnop, D.R., Jimenez, J.L., 2009. Interpretation of organic components from positive matrix factorization of aerosol mass spectrometric data. Atmos. Chem. Phys. 9, 2891–2918.

Vlachou, A., Daellenbach, K.R., Bozzetti, C., Chazeau, B., Salazar, G.A., Szidat, S., et al., 2018. Advanced source apportionment of carbonaceous aerosols by coupling offline AMS and radiocarbon size-segregated measurements over a nearly 2-year period. Atmos. Chem. Phys. 18, 6187–6206.

Vlachou, A., Tobler, A., Lamkaddam, H., Canonaco, F., Daellenbach, K.R., Jaffrezo, J.L., et al., 2019. Development of a versatile source apportionment analysis based on positive matrix factorization: a case study of the seasonal variation of organic aerosol sources in Estonia. Atmos. Chem. Phys. 19, 7279–7295.

WHO, 2006. Air Quality Guidelines: Global Update 2005: Particulate Matter, Ozone, Nitrogen Dioxide and Sulfur Dioxide. World Health Organization, Copenhagen Regional Office for Europe.

WHO, 2018. World Health Organization Mortality Database last updated on 11th April.

WHO, 2021. WHO Global Air Quality Guidelines: Particulate Matter (PM2.5 and PM10), Ozone, Nitrogen Dioxide, Sulfur Dioxide and Carbon Monoxide. World Health Organization, Geneva.

Wu, X., Vu, T.V., Shi, Z., Harrison, R.M., Liu, D., Cen, K., 2018. Characterization and source apportionment of carbonaceous PM2.5 particles in China - a review. Atmos. Environ. 189, 187–212.

Xiao, R., Takegawa, N., Zheng, M., Kondo, Y., Miyazaki, Y., Miyakawa, T., et al., 2011. Characterization and source apportionment of submicron aerosol with aerosol mass spectrometer during the PRIDE-PRD 2006 campaign. Atmos. Chem. Phys. 11, 6911–6929.

Xu, L., Guo, H., Weber, R.J., Ng, N.L., 2017a. Chemical characterization of water-soluble organic aerosol in contrasting rural and urban environments in the southeastern United States. Environ. Sci. Technol. 51, 78–88.

Xu, W., Croteau, P., Williams, L., Canagaratna, M., Onasch, T., Cross, E., et al., 2017b. Laboratory characterization of an aerosol chemical speciation monitor with PM2.5 measurement capability. Aerosol Sci. Technol. 51, 69–83.

Xu, W., He, Y., Qiu, Y., Chen, C., Xie, C., Lei, L., et al., 2020. Mass spectral characterization of primary emissions and implications in source apportionment of organic aerosol. Atmos. Meas. Tech. 13, 3205–3219.

Zhang, Y.L., Perron, N., Ciobanu, V.G., Zotter, P., Minguillón, M.C., Wacker, L., et al., 2012. On the isolation of OC and EC and the optimal strategy of radiocarbon-based source apportionment of carbonaceous aerosols. Atmos. Chem. Phys. 12, 10841–10856.